ACS APPLIED MATERIALS & INTERFACES

Research Article

www.acsami.org

Fabrication, Testing, and Simulation of All-Solid-State Three-Dimensional Li-Ion Batteries

A. Alec Talin,*[,†] Dmitry Ruzmetov,[‡,⊥] Andrei Kolmakov,[‡] Kim McKelvey,[§] Nicholas Ware,[∥] Farid El Gabaly,[†] Bruce Dunn,[∥] and Henry S. White[§]

[†]Sandia National Laboratories, Livermore, California 94551, United States

[‡]Center for Nanoscale Science and Technology, National Institute of Standards and Technology, Gaithersburg, Maryland 20899, United States

[§]Department of Chemistry, University of Utah, Salt Lake City, Utah 84112, United States

[∥]Department of Materials Science and Engineering, University of California, Los Angeles, Los Angeles, California 90095, United States

Supporting Information

ABSTRACT: Demonstration of three-dimensional all-solid-state Li-ion batteries (3D SSLIBs) has been a long-standing goal for numerous researchers in the battery community interested in developing high power and high areal energy density storage solutions for a variety of applications. Ideally, the 3D geometry maximizes the volume of active material per unit area, while keeping its thickness small to allow for fast Li diffusion. In this paper, we describe experimental testing and simulation of 3D SSLIBs fabricated using materials and thin-film deposition methods compatible with semiconductor device processing. These 3D SSLIBs consist of Si microcolumns onto which the battery layers are sequentially deposited using physical vapor deposition. The power performance of the 3D SSLIBs lags significantly behind that of similarly prepared planar SSLIBs. Analysis of the experimental results using finite element modeling indicates that the origin of the poor power performance is the structural inhomogeneity of the 3D SSLIB, coupled with low electrolyte ionic conductivity and diffusion rate in the cathode, which lead to highly nonuniform internal current density distribution and poor cathode utilization.

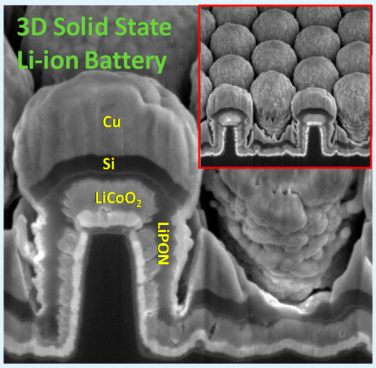

KEYWORDS: *solid-state battery, three-dimensional, thin film, inhomogeneity, experiment and modeling*

INTRODUCTION

Realization of safe, long cycle life, and simple to package solid-state rechargeable batteries with high energy and power density has been a long-standing goal of the energy storage community.[1−3] Much of the research activity has been focused on developing new solid electrolytes with high Li ionic conductivity. Indeed, LiPON, the only solid electrolyte currently used in commercial thin-film solid-state Li-ion batteries (SSLIBs), has a conductivity of $\approx 10^{-6}$ S/cm, compared to ≈0.01 S/cm typically observed for liquid organic electrolytes.[4] Replacing LiPON with a solid electrolyte such as $LiLaTaO_3$ or LiGeSP with an ionic conductivity of $\approx 10^{-3}$ to 10^{-2} S/cm, however, may not improve significantly the power performance of thin-film SSLIBs due to the sluggish Li diffusion in the cathode. For example, in $LiCoO_2$ based thin-film SSLIBs with LiPON electrolyte, the diffusion of Li^+ in the cathode becomes the rate-limiting step for cathode thickness exceeding ≈1 μm.[5] Decreasing the cathode layer significantly below 1 μm is impractical for the thin-film battery since this further reduces the areal charge density from the already low value of ≈0.1 mAh/cm^2. In order to decouple the power density from energy density, numerous proposals have been made to replace the planar, two-dimensional (2D) substrate of the thin-film SSLIB with a 3D scaffolding onto which the battery layers are sequentially deposited.[6] The various proposed 3D SSLIB designs use height (vertical topology) to increase both the electrode surface area and the energy density per geometric footprint. An advantage of the 3D approach is that the anode and cathode substructures can be arranged in close proximity, so that the Li^+ diffusion length during cycling remains short. Furthermore, the increased electrode/electrolyte interfacial area reduces local current density, which in turn leads to lower charge transfer overpotential. Indeed, there are numerous reports of 3D structured electrodes combined with liquid electrolytes that clearly demonstrate the advantages of reduced diffusion length and high interfacial area for high power performance.[2,7,8] However, extending these designs into complete 3D SSLIB with solid electrolytes and with competitive performance characteristics has so far eluded researchers.

In this paper, we demonstrate structural and electrochemical characterization of 3D SSLIBs fabricated using materials and

Received: September 26, 2016
Accepted: November 10, 2016
Published: November 10, 2016

DOI: 10.1021/acsami.6b12244
ACS Appl. Mater. Interfaces 2016, 8, 32385−32391

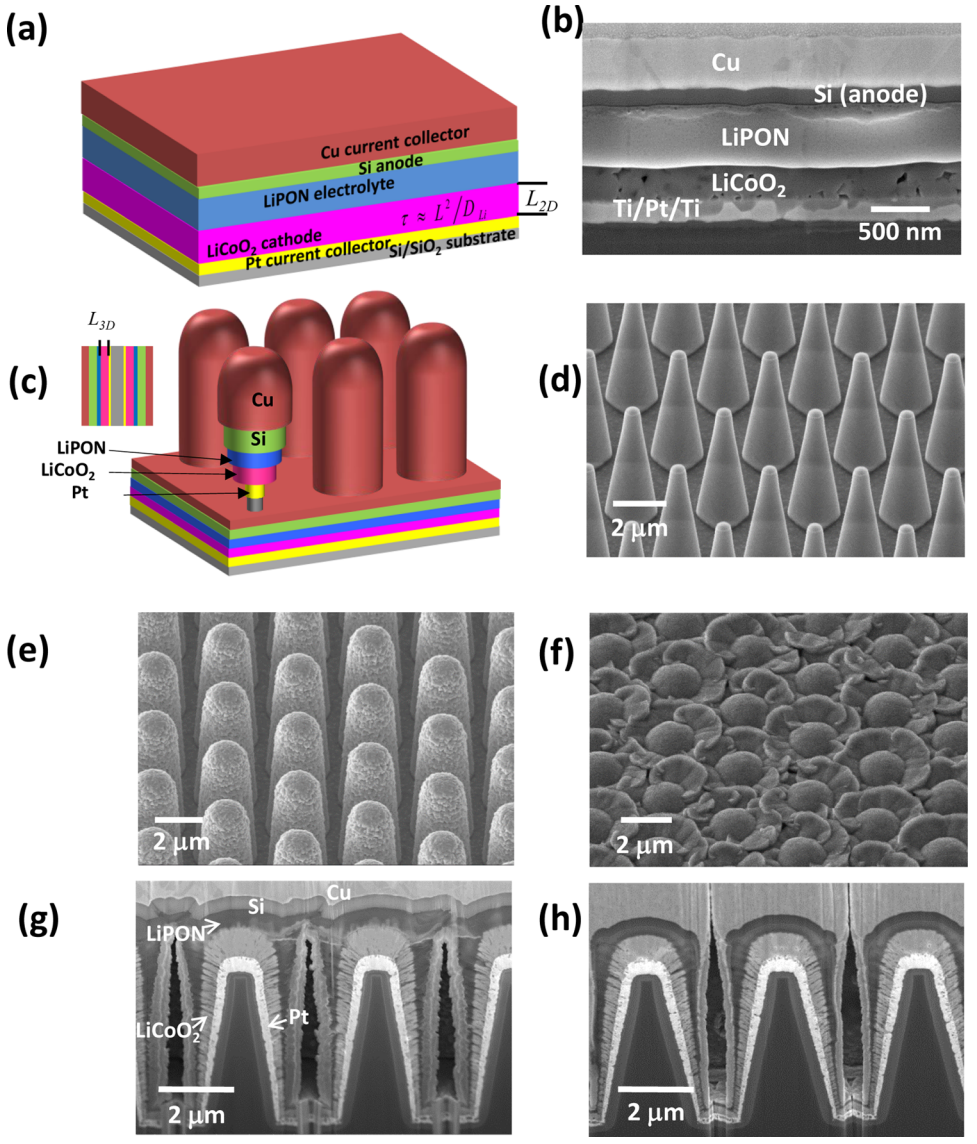

Figure 1. (a) Schematic of a planar thin-film SSLIB. (b) Focused ion beam cross section of a thin-film SSLIB. (c) Schematic of a 3D SSLIB. (d) Si conical microcolumns used as scaffolding for 3D SSLIB. (e) Following Ti/Pt and $LiCoO_2$ deposition. (f) Following LiPON, Si and Cu current collector deposition. (g, h) FIB cross sections of 3D SSLIBs with nominally 500 and 250 nm thick LiPON, respectively.

thin-film deposition methods compatible with semiconductor device processing. We use numerical modeling to relate the structure and performance of the 3D SSLIBs and draw conclusions useful for continued development of high power and high energy density solid-state energy storage devices. Our 3D SSLIBs consist of conical or cylindrical Si microcolumns onto which layers corresponding to the current collector, cathode, electrolyte, and anode are sequentially deposited using physical vapor deposition (PVD). Using galvanostatic charge/discharge cycling, we demonstrate that the power performance of the 3D SSLIBs lags significantly behind that of similarly prepared planar SSLIBs. Analysis of the experimental results using finite element modeling indicates that the origin of the poor power performance is the structural inhomogeneity of the 3D SSLIB, coupled with low electrolyte ionic conductivity, which lead to highly nonuniform internal current density distribution and poor cathode utilization. Our results further confirm that structural uniformity is essential for optimum 3D SSLIB performance and that the existing PVD processes appropriate for planar geometry SSLIBs will likely have to be replaced by alternate processes capable of uniformly coating high aspect ratio microstructures. On the basis of our analysis, we derive a quantitative relationship between the structural inhomogeneity and capacity for different solid electrolyte conductivity values and which can be applied, at least semiquantitatively to a variety of SSLIB and composite electrode designs.

EXPERIMENTAL SECTION

The fabrication process for the planar (2D) batteries has been previously described.[9] Briefly, the process was begun by coating Si(001) substrates capped with 100 nm thick thermal SiO_2 with Ti/Pt (20 nm/120 nm), which serves as the cathode current collector. $LiCoO_2$ (nominal thickness ≈ 300 nm) is then deposited by sputtering in the same system. The samples were then annealed in ambient oxygen at 700 °C for 2 h to form the $LiCoO_2$ high-temperature (HT) phase as determined by Raman spectroscopy.[10] The samples were next sputter-coated with ≈500 nm of LiPON electrolyte at a substrate temperature of 200 °C. The final step consisted of deposition of ≈100 nm of Si, followed by ≈400 nm of Cu current collector using a

DOI: 10.1021/acsami.6b12244
ACS Appl. Mater. Interfaces 2016, 8, 32385−32391

stainless steel shadow mask with an array of 0.5 mm diameter holes to define individual "microbatteries" (see Figure S1a).

The 3D SSLIBs were fabricated using the same procedure on substrates that consisted of arrays of conical Si microcolumns coated with ≈300 nm of SiO_2 (see the Supporting Information for additional fabrication details). The Si conical microcolumns measured 4 μm in height, 1.6 μm diameter at the base, and were positioned with pitch of 3.6 μm. A Si substrate with cylindrical microcolumns was also used for fabricating similar 3D SSLIBs and is shown along with galvanostatic charge/discharge data in the Supporting Information.

The planar SSLIBs were tested using a micromanipulator probe station placed inside an Ar-filled glovebox. The 3D SSLIBs were tested using a custom scanning electron microscope equipped with an electrical micromanipulator probe in order to avoid damaging the microcolumn arrays.[11,12] The testing included galvanostatic charge/discharge cycling at current densities ranging from 2 to 70 $\mu A/cm^2$ and cyclic voltammetry (CV) carried out from 0 to 4 V at a rate of 0.1 mV/s. Additional planar specimens were prepared specifically for EIS measurements, consisting of a planar SSLIB with a $LiCoO_2$ thickness of 200 nm, LiPON thickness of 580 nm, and Si thickness of 50 nm; a companion specimen consisting of 580 nm of LiPON sandwiched between two Au contacts (the LiPON deposited at the same time as the battery) was also fabricated. Electrochemical impedance spectroscopy (EIS) measurements were made using a commercial potentiostat rated for μV and fA precision in sourcing/measuring voltage and current, respectively, with the AC signal frequency varied from 1 Hz to 1 MHz with an amplitude of 25 mV. Note that all deposited layer thicknesses were determined using scanning electron microscopy (SEM) on focused ion beam (FIB) prepared cross sections. The uncertainty (one standard deviation) in the dimensions and thicknesses is estimated to be ≈5% of the value for the planar batteries and ≈10% for the 3D batteries. The electrochemical charge/discharge cycling was performed with high precision instrumentation with 1 fA current sourcing resolution, 1 mV voltage (potential) resolution, and 1 s time resolution, which translated into an accuracy of ±0.02 mAh/cm^2 for charge capacity determination. Nevertheless, because too few planar and 3DSSLIBs were measured in this study to calculate standard deviations, the reported capacities are preceded with the "≈" symbol to indicate that these are approximate values, and that we are mainly concerned with demonstrating and understanding the difference in the capacity measured at different charge rates between the planar and 3D structured solid-state batteries.

Finite element simulations describing the time-dependent nonuniform distributions of Li^+ and the electric potential were used to compute charge and discharge curves for a 3D SSLIB based on the experimental input. Simulations were performed on a desktop PC using a commercial finite element program and are detailed in the Supporting Information.

RESULTS AND DISCUSSION

A schematic of the planar SSLIB and a representative SEM image of a cross section prepared using a focused ion beam (FIB) are shown in Figure 1a,b, respectively. A schematic of an idealized 3D SSLIB and a sequence of three SEM images collected at different stages of fabrication (SiO_2 coated microcolumn array, $LiCoO_2$ deposition, anode deposition) are shown in Figure 1c–f; an FIB prepared cross section of a completed 3D SSLIB is shown in Figure 1g. Additional images for similarly prepared 3D SSLIBs are shown in the Supporting Information. Although the various layers seen in the cross section in Figure 1 were not chemically identified in this study, we previously used multimode analytical scanning/transmission electron microscopy imaging and tomography to characterize in detail the various layers in similarly prepared isolated nanowire SSLIBs.[13]

Inspection of the cross-sectional image shown in Figure 1b with additional images shown in the Supporting Information indicates that the different compositional layers of the planar SSLIB have a relatively uniform thickness and microstructure, closely resembling the intended design depicted in the schematic (Figure 1a). The cross-sectional image in Figure 1g, on the other hand, reveals that the cathode and the electrolyte layers in the 3D SSLIB are highly nonuniform with respect to thickness, and that the anode layer does not conformally cover the microcolumns, as intended in the idealized structure depicted in Figure 1c. Furthermore, the cross-sectional image of the 3D SSLIB shows that the $LiCoO_2$ layer has a distinct columnar morphology on the microcolumn sidewalls. This type of "nanowire" grain morphology is often observed when the substrate is positioned at an oblique angle with respect to the source, a regime referred to as "glancing angle deposition".[14] Transmission electron microscopy analysis of SSLIBs prepared in the same system using a similar procedure on substrates consisting of vertically oriented VLS grown Si microwires revealed that the $LiCoO_2$ grains have a preferred (101) crystallographic orientation along the long grain axis (perpendicular to the metallized Si microcolumn).[13] This orientation of the grain implies a highly anisotropic diffusivity for the Li ions in the cathode, with the faster diffusion occurring perpendicular to the Si microlumn.[13] The LiPON solid electrolyte layer extends to the bottom of the microcolumns and coalesces at the top, leaving an unfilled region in between the microcolumns. No distinct grain structure is evident in the LiPON, consistent with it being amorphous. The coalescence of the electrolyte above the 3D microcolumns forces the Si anode layer to adopt a 2D planar geometry. In an attempt to avoid electrolyte coalescence at the top of the microcolumn array, and thus improve the battery structural uniformity, a 3D SSLIB was fabricated with a thinner LiPON layer (≈250 nm vs ≈500 nm). A cross-sectional image of the resulting 3D SSLIB with the anode and current collector conformally covering the cathode layer down to the base of the array is shown in Figure 1h.

Galvanostatic charge/discharge curves for the planar and 3D SSLIB batteries at different *C*-rates are shown in Figure 2a,b, respectively. (By definition, a 1 *C* rate (h^{-1}) means that the discharge current will discharge the entire battery in 1 h.) The planar SSLIB capacity decreases slightly from ≈21 to ≈18 $\mu Ah/cm^2$ as the rates increase from 7 $\mu A/cm^2$ (0.3 *C*) to 70 $\mu A/cm^2$ (3 *C*). Given a $LiCoO_2$ layer thickness of ≈300 nm in the planar battery, the initial measured discharge capacity represents ≈85% of theoretical the value for $LiCoO_2$ (69 $\mu Ah/cm^2$ per 1 μm thickness). Some Li is known to irreversibly alloy with Si during the first charge cycle, a loss that could be compensated for by lithiating the Si anode during deposition. The slight decrease in capacity with *C*-rate is consistent with the work of Dudney et al., who investigated the effect of increasing thickness of $LiCoO_2$ on power performance of similarly fabricated thin-film SSLIBs.[5]

The capacity for the 3D SSLIB at 0.16 *C* is ≈25 $\mu Ah/cm^2$, slightly higher than the planar SSLIB. In principle, the two types of batteries should have equal capacities (at slow *C*-rate), given that both were coated with the same quantity of $LiCoO_2$ per geometric footprint. However, in contrast to the planar geometry, the capacity of the 3D SSLIB decreases by almost 90%, from ≈23 $\mu Ah/cm^2$ at 0.16 *C* to ≈3 $\mu Ah/cm^2$ at 1.2 *C*. As we demonstrate later in this paper, the dramatic decrease in the apparent capacity of the 3D SSLIB with increasing *C*-rate is due to the large difference in the effective electrolyte thickness for Li^+ insertion/extraction near the top and bottom of the

DOI: 10.1021/acsami.6b12244
ACS Appl. Mater. Interfaces 2016, 8, 32385–32391

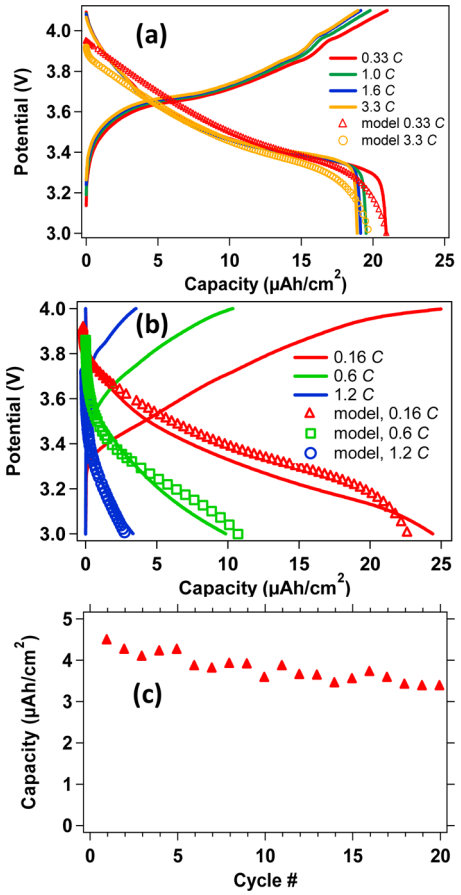

Figure 2. (a) Galvanostatic charge/discharge curves collected for a planar SSLIB; *C*-rates 0.33 *C*, 1 *C*, 1.6 *C*, and 3.3 *C* correspond to discharge current densities 7.1, 21, 34, and 71 μA/cm^2. (b) Galvanostatic charge/discharge curves for the 3D SSLIB along with simulated charge and discharge curves; *C*-rates 0.16 *C*, 0.6 *C*, and 1.2 *C* correspond to 3.7, 13.8, and 27.6 μA/cm^2, respectively. (c) Discharge capacity vs cycle # for 3D SSLIB cycled at 1.2 *C*.

microcolumns as well as slow Li diffusion in the cathode, leading to nonuniform potential distribution and current densities and, hence, highly inhomogeneous charge/discharge rates. Discharge capacity for the 3D SSLIB measured for the first 20 charge/discharge cycles (Figure 2c and Figure S2) demonstrates that the 3D SSLIB can be cycled multiple times and function as a rechargeable battery. The loss in capacity in the first 20 cycles is similar to that we earlier reported for planar SSLIBs fabricated using similar procedure (see Figure 4 in ref 6).

Electrochemical impedance spectroscopy (EIS) was used to estimate the ionic conductivity of the LiPON electrolyte. EIS data for LiPON electrolyte sandwiched between two block (Au) electrodes and a planar SSLIB are shown in Figure S3. An equivalent circuit model consisting of a simplified Randles circuit in series with a constant phase element (CPE) was used to extract a LiPON conductivity of $\approx 2.5 \times 10^{-7}$ S/cm. This conductivity is below the $\approx 10^{-6}$ S/cm value that has been reported for LiPON and could be due to either variation in the deposition process and/or brief exposure of the LiPON to the ambient just prior to anode deposition.[15]

In an effort to improve the structural homogeneity of the 3D SSLIBs, the average electrolyte thickness was decreased, resulting in improved conformal coverage of the anode and current collector, as shown in Figure 1h. However, the 3D SSLIBs with the thinner LiPON could not be charged and discharged due to dielectric breakdown of the electrolyte. Dielectric breakdown occurs when the electric field in the electrolyte exceeds a critical value, typically >10^5 V/cm, resulting in large electronic current between the anode and the cathode.[16] Cyclic voltammetry data (Figure 3) show that

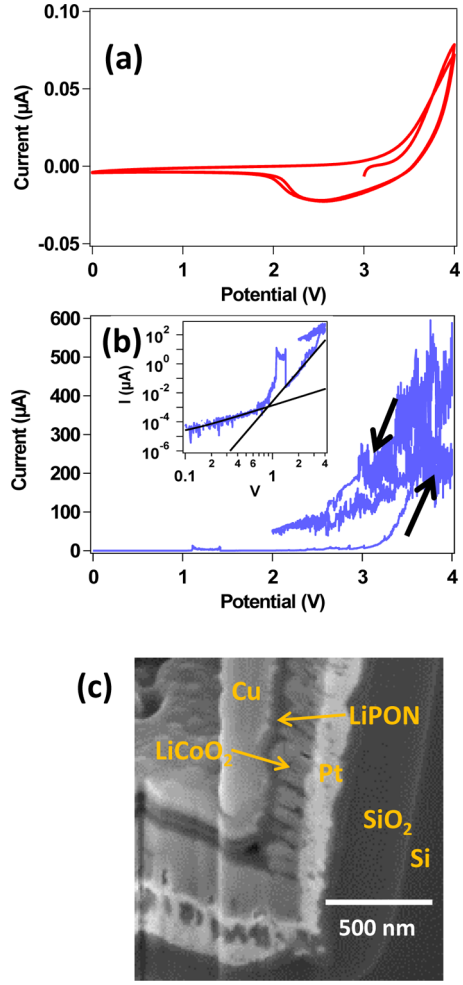

Figure 3. (a) Cyclic voltammetry measured for the 3D SSLIB with nominally 500 nm thick LiPON (shown in Figure 1g). (b) Cyclic voltammetry for the 3D SSLIB with nominally 250 nm thick LiPON (shown in Figure 1h). (c) SEM image of the bottom corner of 3D SSLIB that exhibits dielectric breakdown.

the 3D SSLIB with the thicker electrolyte displays positive and negative currents during charge and discharge, respectively, while the battery with the thinner LiPON shows *only* positive current and with much higher magnitude (tens of nanoamps vs hundreds of microamps). Analysis of the current–voltage data on a log–log plot (inset, Figure 3b) for the thinner LiPON battery suggests that electron transport is by a trap-assisted space-charge limited mechanism, characterized by increased slope at higher bias and considerable hysteresis, closely resembling memristors.[16] The likely reason for dielectric breakdown is the very thin anode–cathode separation regions (<30 nm) formed near the bottoms of the microcolumns, as shown in Figure 3c. The combination of very thin electrolyte and high aspect ratio cathode morphology (due to the glancing angle deposition regime) leads to enhanced local electric fields

DOI: 10.1021/acsami.6b12244
ACS Appl. Mater. Interfaces 2016, 8, 32385–32391

that can easily exceed the dielectric breakdown strength of the electrolyte. Defect states or traps lying somewhere in the energy gap of the LiPON electrolyte could be ionized at sufficiently high fields, leading to electronic current injection and breakdown.

The experimental results qualitatively suggest that lack of structural homogeneity coupled with low solid electrolyte conductivity leads to the poor 3D SSLIB performance. This explanation is further supported experimentally by EIS measurements shown in Figure S2. The overall magnitude of the SSLIB impedance is almost equal to that of the LiPON, indicating that bulk electrolyte transport, rather than interfacial charge transport, dominates the internal battery resistance, at least at low *C*-rates. This result is consistent with a recent report of extremely low interfacial resistance measured for $LiCoO_2$/LiPON interfaces where damage by N atoms during sputtering was minimized.[17]

We developed a finite element model of the 3D SSLIB in order to gain a deeper understanding of how the nonplanar battery geometry, coupled with the low solid-state electrolyte conductivity, affects the power capability. Details of the computation model are presented in the Supporting Information. An idealized 2D axial symmetric geometry was defined based on the conical shape elements of the 3D SSLIB cross-sectional image, as depicted in Figure 4. Both diffusion

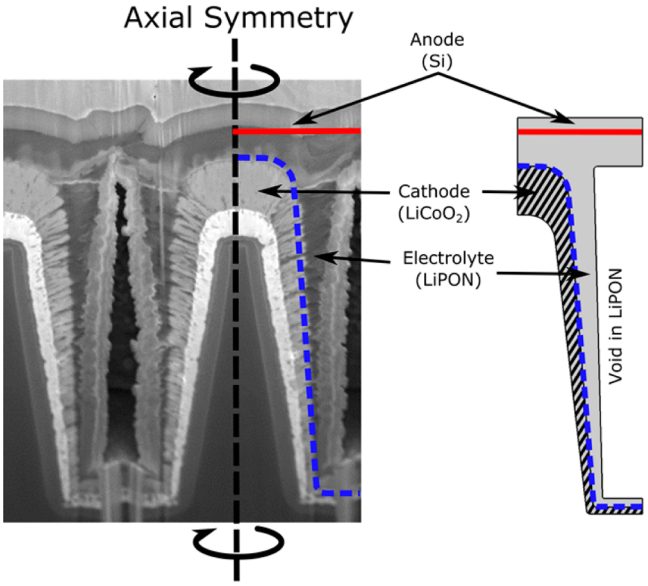

Figure 4. 2D axial symmetric geometry used in the finite element model defined based on the conical shape elements of the 3D SSLIB cross-sectional image. The anode/electrolyte boundary is shown as a red line, while the cathode/electrolyte boundary is shown as a blue dotted line.

and migration of Li ions was simulated within the LiPON electrolyte, while the transport of Li ions within the $LiCoO_2$ cathode and the Si anode was assumed to occur only by diffusion. Within the LiPON electrolyte, a counterion, x^-, with a charge of −1, which does not transfer across the anode/electrolyte or cathode/electrolyte boundaries but has a mobility equal to that of Li ions, was used to maintain electroneutrality.[18] In addition, the diffusion within the $LiCoO_2$ cathode was anisotropic, with the diffusion along the surface significantly reduced compared to the diffusion normal to the surface due to the columnar nature of the $LiCoO_2$.

Li-ion transfer across both the anode/electrolyte and the cathode/electrolyte interfaces (as shown in Figure 4) was modeled using potential-dependent Butler−Volmer (BV) kinetic expressions. Importantly, the use of BV kinetics means that the insertion/extraction rate of Li ions at any point along the electrode/electrolyte interfaces depends on the local concentration of Li ions as well as the local activation overpotential, the latter varying dramatically during discharge/charge due to variation in the potential drop resulting from the lack of a conformal electrolyte layer.

First, we consider the simulated discharge over a range of different rates corresponding to the experimental rates. The resulting simulated cell potential vs capacity for the planar and the 3D SSLIB discharge with a LiPON conductivity of 2.5×10^{-7} S/cm are shown in Figure 2a,b, respectively. In the planar geometry, an increase in the charge/discharge rate by a factor of ≈10 (0.3 *C* to 3.3 *C* in Figure 2a) results in an 11% loss in capacity in the simulation as compared to a 9% loss in capacity that is observed experimentally. Meanwhile, in the 3D geometry, a 7.5 fold increase in the charge/discharge rate (0.16 *C* to 1.2 *C* in Figure 2b) results in an 87% loss in capacity in the simulations, compared to a similar 90% loss of capacity observed experimentally.

We next consider the dynamics of Li-ion transport during a 1.2 *C* charge from an initial uniform Li-ion concentration in order to illustrate the mechanism responsible for poor battery performance of the 3D SSLIB. The concentration profiles at three snapshots during a 1.2 *C* rate charge are shown in Figure 5a, (i) at the start of the charge cycle at $t = 0$ s, (ii) halfway through the charge at $t = 240$ s, and (iii) at the end of the charge $t = 480$ s. At the start of the charge cycle, the Li-ion concentration is uniform, but as the charge proceeds (Figure 5, $t = 240$ s and $t = 480$ s), Li^+ is transported from the anode to the cathode. This transport decreases the local concentration of Li^+ in the electrolyte near the anode/electrolyte (as seen in red near the anode boundary in Figure 5a at $t = 240$ s and $t = 480$ s) while increasing the local concentration of Li^+ in the electrolyte at the cathode/electrolyte boundary (as seen as darker blue near the cathode boundary in Figure 5a at $t = 240$ s and $t = 480$ s). The local concentration of Li^+ within the cathode near the cathode/electrolyte boundary also decreases (as seen as red near the cathode boundary in Figure 5a at $t = 240$ s and $t = 480$ s). However, due to the nonuniform electrolyte thickness (i.e., the nonuniform distance between the cathode and the anode), the Li^+ increase in the electrolyte (and a corresponding decrease in Li^+ in the cathode) occurs principally at the top of the microcolumns (at the point of the shortest distance between the anode and the cathode). This preferential saturation of Li^+ in the electrolyte (and depletion of Li^+ in the cathode) near the cathode/electrolyte interface at the top of the microcolumns has the subsequent effect of reducing the local flux of Li^+ across the cathode/electrolyte boundary at the top of the microcolumn. As the charge proceeds, the transport of Li^+ across the cathode/electrolyte interface is forced further down the microcolumns, introducing a larger potential drop across the electrolyte due to its finite conductance, as shown with the progression of solution potential in Figure 5b. This compares to the small concentration and potential gradients that develop in the planar SSLIB geometry at a comparable 1.2 *C*-rate, which are shown in Figure 5c. The depletion/saturation of the cathode interface in the nonuniform geometry, coupled with the finite electrolyte, reduces the performance of the battery. In addition,

DOI: 10.1021/acsami.6b12244
ACS Appl. Mater. Interfaces 2016, 8, 32385−32391

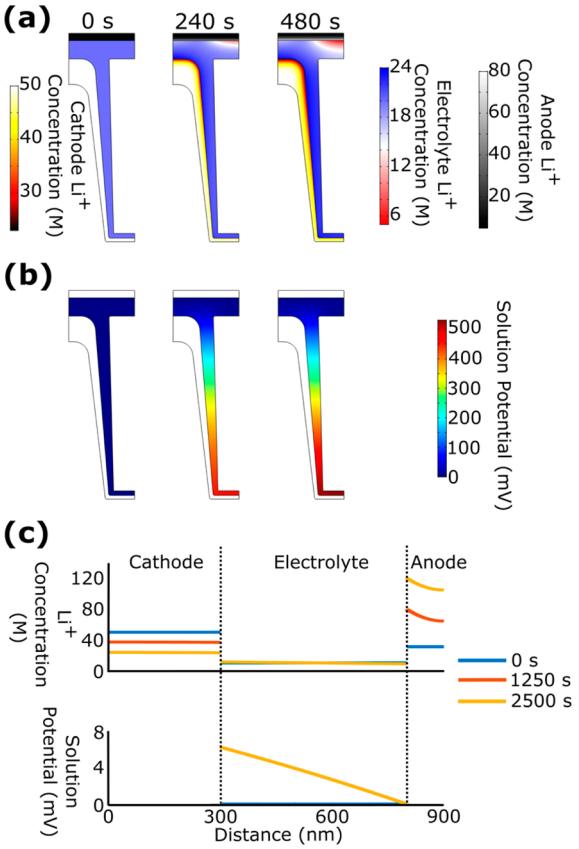

Figure 5. Concentration (a) and potential (b) profiles for three time points (0, 240, and 480 s) during a 1.2 *C*-rate charge from an initially uniform Li^+ concentration for the 3D SSLIB. (c) Li^+ concentration and potential profiles at three time points (0, 1250, and 2500 s) during a 1.2 *C*-rate charge in a planar SSLIB from an initial uniform profile.

the slow diffusion of Li^+ within the cathode reduces the capacity and results in underutilizing the cathode material. Taken together, these simulations show that cell performance is limited by the nonuniform distance between the anode and the cathode in combination with the limited Li^+ transport in both the electrolyte and the cathode. Simulations would suggest that cell performance can be improved by increasing the conductivity of the LiPON electrolyte, increasing the diffusion of Li^+ in the cathode, or by changing the geometry of the 3D SSLIB to have a constant distance between the anode and the cathode (constant thickness electrolyte).

CONCLUSION

In summary, we have demonstrated rechargeable 3D solid-state Li-ion batteries with microscale internal dimensions, fabricated using materials and thin-film deposition methods compatible with semiconductor device processing. We have shown that the power performance of these 3D SSLIBs lags significantly behind that of similarly prepared planar batteries, and that the origin of this poor power performance is the combination of structural inhomogeneity of the 3D SSLIB with low electrolyte ionic conductivity. Together, the inhomogeneity and low electrolyte conductivity lead to a highly nonuniform internal current density distribution and poor cathode utilization. However, increasing the electrolyte conductivity to 10^{-5} S/cm would allow a 3D SSLIB to maintain (with a less than 1% loss in capacity) the superior performance compared to planar batteries, even with an inhomogeneity ratio (the ratio of the longest to shortest path from the anode to the cathode) of 0.2, as shown in Figure S7.

ASSOCIATED CONTENT

Supporting Information

The Supporting Information is available free of charge on the ACS Publications website at DOI: 10.1021/acsami.6b12244.

Additional fabrication details and Raman spectrum of $LiCoO_2$; cross-sectional SEM and cycling data for 3D SSLIB with different microcolumn dimensions; EIS data and analysis for LiPON electrolyte and planar SSLIB; and details of finite element model and additional simulation results (PDF)

AUTHOR INFORMATION

Corresponding Author

*E-mail: aatalin@sandia.gov.

ORCID

A. Alec Talin: 0000-0002-1102-680X

Dmitry Ruzmetov: 0000-0002-0688-1908

Present Address

⊥U.S. Army Research Laboratory, Adelphi, MD.

Notes

The authors declare no competing financial interest.

ACKNOWLEDGMENTS

A.A.T., K.M., N.W., F.E.G., B.D., and H.S.W. were supported by the Science of Precision Multifunctional Nanostructures for Electrical Energy Storage (NEES), an Energy Frontier Research Center funded by the U.S. DOE, Office of Science, Office of Basic Energy Sciences, under award DESC0001160. The authors acknowledge CNST NIST NanoFab personnel for help in fabrications and tests of the 3D batteries. D.R. acknowledges support under the Cooperative Research Agreement between the University of Maryland and the National Institute of Standards and Technology Center for Nanoscale Science and Technology, Award 70NANB10H193, through the University of Maryland. Sandia National Laboratories is a multiprogram laboratory managed and operated by Sandia Corporation, a wholly owned subsidiary of Lockheed Martin Corporation, for the U.S. Department of Energy's National Nuclear Security Administration under contract DE-AC04-94AL85000.

REFERENCES

(1) Baggetto, L.; Niessen, R. A. H.; Roozeboom, F.; Notten, P. H. L. High Energy Density All-Solid-State Batteries: A Challenging Concept Towards 3D Integration. *Adv. Funct. Mater.* **2008**, *18* (7), 1057−1066.

(2) Ferrari, S.; Loveridge, M.; Beattie, S. D.; Jahn, M.; Dashwood, R. J.; Bhagat, R. Latest Advances in the Manufacturing of 3D Rechargeable Lithium Microbatteries. *J. Power Sources* **2015**, *286*, 25−46.

(3) Long, J. W.; Dunn, B.; Rolison, D. R.; White, H. S. Three-Dimensional Battery Architectures. *Chem. Rev.* **2004**, *104* (10), 4463−4492.

(4) Bachman, J. C.; Muy, S.; Grimaud, A.; Chang, H.-H.; Pour, N.; Lux, S. F.; Paschos, O.; Maglia, F.; Lupart, S.; Lamp, P.; Giordano, L.; Shao-Horn, Y. Inorganic Solid-State Electrolytes for Lithium Batteries: Mechanisms and Properties Governing Ion Conduction. *Chem. Rev.* **2016**, *116* (1), 140−62.

(5) Dudney, N. J.; Jang, Y. I. Analysis of Thin-film Lithium Batteries with Cathodes of 50 nm to 4 μm Thick $LiCoO_2$. *J. Power Sources* **2003**, *119*−*121*, 300−304.

DOI: 10.1021/acsami.6b12244
ACS Appl. Mater. Interfaces 2016, 8, 32385−32391

(6) Notten, P. H. L.; Roozeboom, F.; Niessen, R. A. H.; Baggetto, L. 3-D Integrated All-Solid-State Rechargeable Batteries. *Adv. Mater.* **2007**, *19* (24), 4564−4567.
(7) Xia, H.; Wan, Y. H.; Assenmacher, W.; Mader, W.; Yuan, G. L.; Lu, L. Facile Synthesis of Chain-like $LiCoO_2$ Nanowire Arrays as Three-Dimensional Cathode for Microbatteries. *NPG Asia Mater.* **2014**, *6*, e126.
(8) Xia, H.; Xia, Q.; Lin, B.; Zhu, J.; Seo, J. K.; Meng, Y. S. Self-standing porous $LiMn_2O_4$ Nanowall Arrays as Promising Cathodes for Advanced 3D Microbatteries and Flexible Lithium-ion Batteries. *Nano Energy* **2016**, *22*, 475−482.
(9) Gong, C.; Ruzmetov, D.; Pearse, A.; Ma, D. K.; Munday, J. N.; Rubloff, G.; Talin, A. A.; Leite, M. S. Surface/Interface Effects on High-Performance Thin-Film All-Solid-State Li-Ion Batteries. *ACS Appl. Mater. Interfaces* **2015**, *7* (47), 26007−26011.
(10) Baddour-Hadjean, R.; Pereira-Ramos, J. P. Raman Microspectrometry Applied to the Study of Electrode Materials for Lithium Batteries. *Chem. Rev.* **2010**, *110* (3), 1278−1319.
(11) Talin, A. A.; Leonard, F.; Katzenmeyer, A. M.; Swartzentruber, B. S.; Picraux, S. T.; Toimil-Molares, M. E.; Cederberg, J. G.; Wang, X.; Hersee, S. D.; Rishinaramangalum, A. Transport Characterization in Nanowires Using an Electrical Nanoprobe. *Semicond. Sci. Technol.* **2010**, *25* (2), 024015.
(12) Leite, M. S.; Ruzmetov, D.; Li, Z. P.; Bendersky, L. A.; Bartelt, N. C.; Kolmakov, A.; Talin, A. A. Insights into Capacity Loss Mechanisms of All-Solid-State Li-ion Batteries with Al Anodes. *J. Mater. Chem. A* **2014**, *2* (48), 20552−20559.
(13) Oleshko, V. P.; Lam, T.; Ruzmetov, D.; Haney, P.; Lezec, H. J.; Davydov, A. V.; Krylyuk, S.; Cumings, J.; Talin, A. A. Miniature All-Solid-State Heterostructure Nanowire Li-ion Batteries as a Tool for Engineering and Structural Diagnostics of Nanoscale Electrochemical Processes. *Nanoscale* **2014**, *6* (20), 11756−11768.
(14) Zhao, Y. P.; Ye, D. X.; Wang, G. C.; Lu, T. M. Novel Nano-Column and Nano-Flower Arrays by Glancing Angle Deposition. *Nano Lett.* **2002**, *2* (4), 351−354.
(15) Yu, X. H.; Bates, J. B.; Jellison, G. E.; Hart, F. X. A Stable Thin-Film Lithium Electrolyte: Lithium Phosphorus Oxynitride. *J. Electrochem. Soc.* **1997**, *144* (2), 524−532.
(16) Ruzmetov, D.; Oleshko, V. P.; Haney, P. M.; Lezec, H. J.; Karki, K.; Baloch, K. H.; Agrawal, A. K.; Davydov, A. V.; Krylyuk, S.; Liu, Y.; Huang, J. Y.; Tanase, M.; Cumings, J.; Talin, A. A. Electrolyte Stability Determines Scaling Limits for Solid-State 3D Li Ion Batteries. *Nano Lett.* **2012**, *12* (1), 505−511.
(17) Haruta, M.; Shiraki, S.; Suzuki, T.; Kumatani, A.; Ohsawa, T.; Takagi, Y.; Shimizu, R.; Hitosugi, T. Negligible "Negative Space-Charge Layer Effects" at Oxide-Electrolyte/electrode Interfaces of Thin-Film Batteries. *Nano Lett.* **2015**, *15* (3), 1498−1502.
(18) Danilov, D.; Niessen, R. A. H.; Notten, P. H. L. Modeling All-Solid-State Li-Ion Batteries. *J. Electrochem. Soc.* **2011**, *158* (3), A215−A222.

DOI: 10.1021/acsami.6b12244
ACS Appl. Mater. Interfaces 2016, 8, 32385−32391